使用により、リウマチや骨粗鬆症など、良好な移植骨が得られない症例でも骨再生が可能となった。

1.5 自家骨髄培養細胞導入人工骨による骨再生医療

上記臨床例では良好な成果を示したが、NEOBONE単独で使用可能なのは骨再生条件の良好な比較的小さな骨欠損に限られる。感染による骨欠損、偽関節、腫瘍による高度骨欠損などの骨形成条件の悪い部位にはNEOBONE単独での骨移植では不十分で、NEOBONE自体に骨形成能を有するBio-Active NEOBONE（培養骨）が必要と考えられる。大阪大学医学部附属病院に新設された未来医療センターのプロジェクトとして「自家骨髄由来培養細胞導入人工骨による骨疾患の治療—第Ⅰ/Ⅱ相臨床試験」を開始した[15]。未来医療センターは再生医療や遺伝子治療などの臨床プロジェクトについて、プロトコール作製・支援、医学的評価、倫理的・社会的評価を経て系統的に推進し、有効性・安全性・経済性などについて客観性の高い分析を支援している。対象は長径30 mm以上の良性骨腫瘍の20歳以上の患者で、①患者から200～800 mLの末梢血を採取し遠心分離にて血清を分離、②外来処置にて骨髄穿刺を行い骨髄液15～50 mLを採取、③未来医療センター内に設置された細胞調整施設（Cell Processing Center；CPC）において、骨髄細胞を自己血清を用いて培養増幅し（初期培養）、NEOBONEの気孔内に導入して骨芽細胞への分化誘導培養（2次培養）を行い、④合計4～6週の培養後、最終製品である“培養骨”を手術室に搬送し、良性骨腫瘍の掻爬術で生じた骨欠損に移植している。

1.6 おわりに

近年、種々の人工骨の開発が進められ骨の再生医学への臨床応用が期待されている。今回開発したNEOBONEの使用により、連通気孔構造を利用して骨髄幹細胞やBMP等のサイトカインを気孔内に容易に導入することが可能となった。BMPの生物活性をさらに有効に利用し、骨再生をさらに促進できるものと考える。また臨床でのBMPの使用量を減少できる可能性が示された。NEOBONEは単独使用においても良好な結果を示したが、血管の導入や自己骨髄細胞を導入した生体活性型人工骨が臨床応用されれば、これまで困難であった難治性骨関節疾患の治療に貢献できることを期待する。今後、組織工学、分子生物学のさらなる進歩により、先端医療としての骨組織のTissue Engineeringが可能になるものと思われる。

文献

1) Yoshikawa H, et al: Clinical application of calcium hydroxyapatite ceramic in bone tumor surgery. Wise DL ed: Biomaterials and Bioengineering Handbook, Marcel Dekker, New York, p433-455, 1999
2) Matsumine A, et al: Calcium hydroxyapatite ceramic implants in bone tumor surgery. A long-term follow-up study. J Bone Joint Surg **86B**: 719-725, 2004
3) Nishikawa M, et al: Calcium phosphate ceramics in Japan. Yaszemski MJ, et al ed: Biomaterials in Orthopedics, Marcel Dekker, New York, p425-436, 2004
4) Tamai N, et al: Novel hydroxyapatite ceramics with an interconnective porous structure exhibit superior osteoconduction in vivo. J Biomed Mater Res **59**: 110-117, 2002
5) 吉川秀樹ほか：骨組織再生の促進。整形外科の最新医療、先端医療技術研究所、東京、p45-48, 2003
6) Myoui A, et al: Three-dimensionally engineered hydroxyapatite ceramics with interconnected pores as a bone substitute and tissue engineering scaffold. Yaszemski MJ, et al ed: Biomaterials in Orthopedics, Marcel Dekker, New York, p287-300, 2004
7) Ohgushi H, et al: Stem cell technology and bioceramics: from cell to gene engineering. J Biomed Mater Res **48**: 913-927, 1999
8) Nishikawa M, et al: Bone tissue engineering using novel interconnected porous hydroxyapatite ceramics combined with marrow mesenchymal cells: Quantitative and three-dimensional image analysis. Cell Transplantation **13**: 367-376, 2004
9) Saito N, et al: Biodegradable poly, -lactic acid-polyethyleue glycol block copolymers as a BMP delivery system for inducing bone. J Bone Joint Surg **83A**: S92-98, 2001
10) Kaito T, et al: Potentiation of the activity of bone morphogenetic protein-2 in bone regeneration by a PLA-PEG/hydroxyapatite composite. Biomaterials **26**: 73-79, 2005
11) Akita S, et al: Capillary vessel network integration by inserting a vascular pedicle enhances bone formation in tissue-engineered bone using interconnected porous hydroxyapatite ceramics. Tissue Engineering **10**: 789-795, 2004
12) Tamai N, et al: A new biotechnology for articular cartilage repair: subchondral implantation of a composite of interconnected porous hydroxyapatite, synthetic polymer (PLA/PEG), and bone morphogenetic protein-2(rhBMP-2). Osteoarthritis Cartilage **13**: 405-417, 2005
13) 玉井宣行ほか：新規全気孔連通型HA多孔体NEOBONEを用いた骨欠損に対する治療。関節外科 **23**: 100-107, 2004
14) 玉井宣行ほか：人工骨材料と骨・関節修復。分子リウマチ **1**: 107-112, 2004
15) 名井　陽ほか：連通多孔体型ハイドロキシアパタイトの開発と再生医療への展開。骨・関節・靭帯 **17**: 1205-1215, 2004

（吉川秀樹、名井　陽）

理学療法学　第32巻第8号　441～444頁（2005年）

特別講演

運動器の再生医療の現状と展望*

吉川秀樹**

はじめに

2000年より始まった“骨関節の10年（Bone and Joint Decade）”政策に伴い，世界的に運動器疾患に対する積極的な研究推進が図られている。この世界運動の対象は，関節疾患，脊椎疾患，骨粗鬆症，重度外傷，小児運動器障害が挙げられており，この10年間の達成目標は，以下の4点である。1. 運動器障害の実態を調査し，患者，家族，社会や経済に及ぼす負担を把握し，社会に知ってもらう。2. 患者や市民に自らの健康管理について，より積極的に参加してもらう。3. 質の高い，経済効率の良い医療・予防法を広く実施する。4. より本質的な治療・予防法を開発するための基礎的研究を推進する。このような世界運動の中で，近年，特に問題となっているのは，高齢化に伴い，変形性関節症，骨粗鬆症による大腿骨頸部骨折，脊椎圧迫骨折が増加していることである。変形性関節症に対しては，人工関節による手術が普及してきたが，その耐久性には，未だ問題があること，人工関節近傍の骨が脆弱なため，人工関節のゆるみや，骨折などをしばしば惹起する。また，骨の感染や腫瘍切除後の大きな骨の欠損部の修復にも骨再生医療が必要である。一方，スポーツの普及による関節軟骨損傷や加齢に伴う関節軟骨の変性・破綻に対しては，軟骨の再生医療が必要である。軟骨は，本来再生能力が乏しいため，再生のためには軟骨細胞や骨髄幹細胞の導入が必要で，コラーゲンなどの担体を用いた軟骨の再生が試みられている。その他，腱，靭帯，半月板，神経など運動器の再生医療のための基礎的研究が進められている。本稿では，骨，軟骨，半月板の再生を中心に，運動器の再生医療の現状と将来展望について概説する。

骨の再生

骨組織は，骨折の治癒現象に代表されるように，本来豊かな再生能力を有しており，創外固定器による脚延長や変形矯正により，骨を再生させる技術が進歩してきた。しかし，骨腫瘍の切除後や，重度の粉砕骨折などで生じた大きな骨欠損に対しては，自家骨では対応できず，骨の再生医療が必要となる。また，骨折や骨欠損の早期の修復のためには，幹細胞移植や増殖／分化因子による骨形成促進を併用する必要がある。骨は力学的強度を必要とする組織であり，その再生／修復には，骨形成細胞の足場としての良好なバイオマテリアルの開発と，間葉系細胞や骨芽細胞の増殖・分化の促進の両面から研究が進んでいる。骨は力学的強度が必要であり，その再生には，骨が形成される足場としての良好な人工骨の開発が必要である。近年，ハイドロキシアパタイトセラミック（HA）などの優れた人工骨が開発され，自家骨移植に代わって広く使用されつつある[1)2)]。著者らは，力学的強度を有し，かつ幹細胞や骨増殖因子の導入が可能な骨補填材料として，気孔間連通構造を有する新規ハイドロキシアパタイトを開発した[3)]。“起泡ゲル化技術”による新規多孔体人工骨（NEOBONE）は，ほぼ球形で比較的均一のサイズの気孔が秩序良く配列し，ほぼ全気孔が気孔間連通孔で連絡している（図1）。連通孔径分布は10～80 μm（平均40 μm）にあり，気孔の90％が細胞や組織が十分通過できる大きさの連通孔でつながっており，気孔の内部に骨髄幹細胞，血管，骨形成蛋白（BMP）などの増殖因子／サイトカインや遺伝子の導入が可能である。実際，この気孔の内部にラット骨髄幹細胞を注入し，任意の部位に骨形成を惹起することに成功している[4)]（図2）。力学的強度は初期圧縮強度で10 Mpa以上であり優れた数値を示した。ウサギ大腿骨にNEOBONEを移植した際に，移植後わずか6週間で直径6 mmの円柱の深層にまで気孔間連通孔を経て，豊富な血管新生を伴う，新生骨，新生骨髄が観察され，優れた骨再生能を示した。現在，血管[5)]やBMP[6)]を導入し（図3），さらなる骨再生の促進を試みており，近い将来，先端医療としての，骨組織のTissue Engineeringが可能になるものと思われる。現在，このNEOBONEは，厚生労働省の認可を得，広く医療現場で使用されている。自家骨を採取することなく，NEOBONE単独で，種々の骨欠損部の

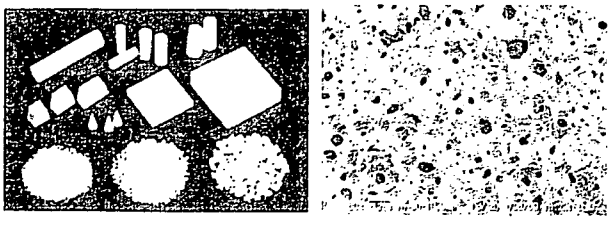

図1　骨再生のための新規人工骨（NEOBONE）（左：肉眼像，右：走査電顕像での内部気孔と連通孔）

---

* Regenerative Medicine of the Musculoskeletal System: Current Status and Perspective

** 大阪大学大学院医学系研究科器官制御外科学（整形外科）
（〒565-0871 大阪府吹田市山田丘2-2）
Hideki Yoshikawa, MD, PhD: Department of Orthopaedic Surgery, Osaka University Graduate School of Medicine

キーワード：骨再生，人工骨，再生医療

図2 ラット骨髄幹細胞とNEOBONE複合体を筋肉内移植後4週の骨形成

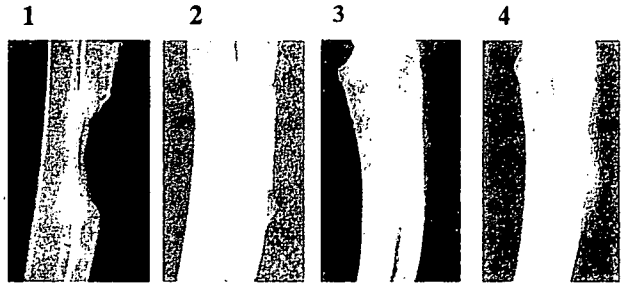

図3 NEOBONEと骨形成蛋白（BMP）によるウサギ前腕骨欠損部の再生（1：欠損のみ，2：NEOBONEのみ，3：NEOBONE/BMP 5 μg，4：NEOBONE/BMP 20 μg）（移植後5週）

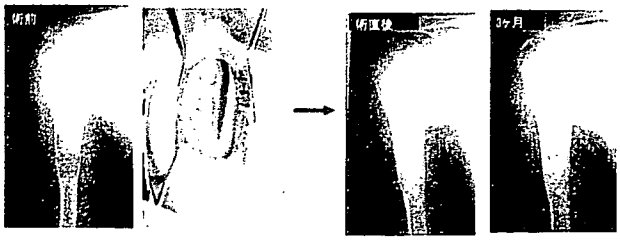

図4 良性骨腫瘍の骨再生（14歳，男子，右上腕骨骨のう腫）

再生に臨床応用している。骨腫瘍による骨欠損部に対しては，NEOBONEにより良好な治療成績が得られている（図4）。また，高位脛骨骨切り術に対する骨接合のため，3次元コンピューターシミュレーションを用いて術前にNEOBONEを成型し，使用している（図5）。また，関節近傍の骨嚢腫がある症例では，まずNEOBONEを移植し母床骨を再生させ，2期的に人工関節を設置している（図6）。関節リウマチ患者の人工関節のゆるみによる広範囲の骨欠損に対しても，同様のシミュレーションを用いて，骨欠損部の補填を行い，自家骨移植なしで，良好な骨癒合を得ている（図7）。

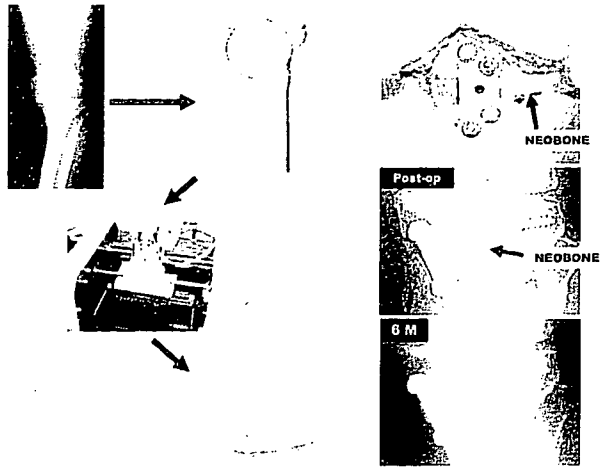

図5 高位脛骨骨切り術（62歳，女性，左変形性膝関節症）

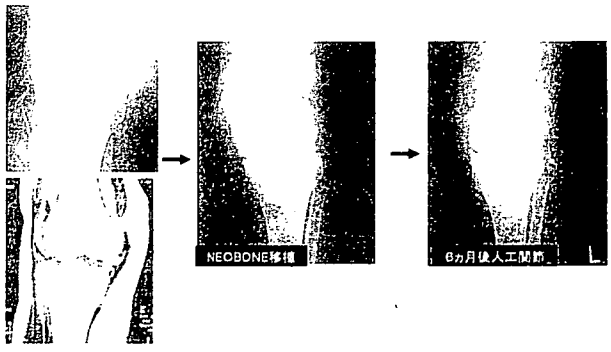

図6 関節近傍の骨再生後の人工関節設置例（65歳，女性，関節リウマチ）

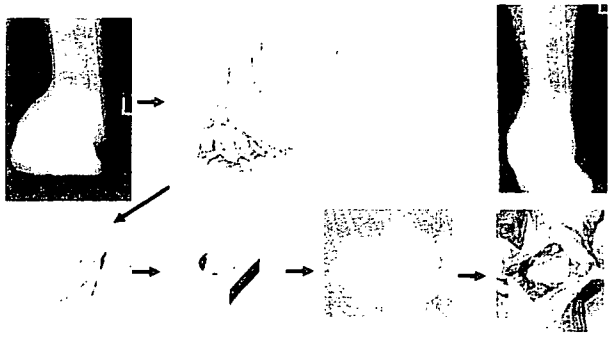

図7 人工関節ゆるみによる広範骨欠損に対する関節固定術（72歳，女性，関節リウマチ）

軟骨の再生

近年のスポーツ人口の増加に伴い，膝関節軟骨損傷例が著しく増加している。これら若年者―成人の軟骨損傷に対しては，骨髄幹細胞の導入のための骨孔作成（ドリリング）や，健常部の骨軟骨柱を採取し，欠損部に移植するという自家骨軟骨移植術などの治療が行われている[7]（図8）。しかし，小さい軟骨欠損部に対しては，良好な成績が得られているものの，大きな軟骨損傷や，変形性関節症による高齢者の軟骨変性の修復には，これらの方法では対応できないのが現状である。関節軟骨の修復能力は骨と比較し著しく劣り，成人では，完全な硝子軟骨で

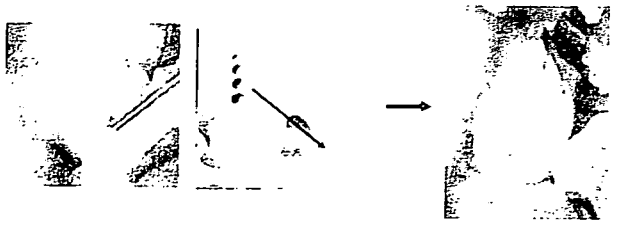

図8　自家骨軟骨移植術（左：術前，右：術後）

修復されることは考えにくい。その理由の一つとしては，欠損部に供給される前駆細胞数が十分でないことが考えられる。従って，軟骨再生には，軟骨細胞や骨髄幹細胞を用いた種々Tissue Engineeringの試みがなされてきた。

1. 自家軟骨細胞移植による関節軟骨の再生

米国Genzyme社は，1997年，整形外科分野での関節軟骨の再生を目指した自家軟骨細胞培養・移植法を開発し，FDAの認可を受け商品化した（Carticel®）。実際には，各医療施設において，膝関節損傷患者に対し，関節鏡視下に非荷重部から軟骨組織を採取する。軟骨組織は，ボストンのGenzyme社に送られ，酵素処理により消化され，軟骨細胞が分離・培養される。約3週後に，元の医療施設に返送され，同患者さんに移植手術が行われるシステムである[8]。欠損部の変性した軟骨を除去し，脛骨前面より採取した骨膜を欠損部に縫着し，骨膜下に軟骨細胞を注入する方法である。累積移植患者数は5000例を超えており，臨床評価としてはある程度の良好な成績が報告されている。現在，本邦でも同様の手法で臨床試験が開始されている。しかし，臨床評価のみで，MRIなどによる客観的評価が十分になされていないこと，感染のリスク，医療費の問題など検討すべき問題点が残されている。

2. 自家軟骨細胞や骨髄間葉系細胞移植による関節軟骨の再生

ウサギの関節軟骨細胞を採取し，in vitroで増殖させた後，I型コラーゲン・ゲル内に埋植し，大腿骨内顆荷重部に作成した6×3×3mmの骨軟骨欠損部に充填した。移植後2週間で，移植細胞は軟骨に分化し，骨軟骨欠損部全域が軟骨に再生した。24週間後には，軟骨下骨は完全に修復され，関節軟骨は，軟骨として残存した[9]（図9）。一方，骨髄あるいは骨膜に存在する間葉系細胞中には，軟骨前駆細胞が含まれている。そこで，十分な前駆細胞を軟骨欠損部に供給するために，骨髄間葉系細胞をin vitroで増殖させ，軟骨欠損部に移植し，軟骨再生を促進できる可能性がある。現在，変形性膝関節症患者に対し臨床試験が試みられている。すなわち，高位脛骨骨切術の手術後3週間前に，本人の腸骨から，骨髄細胞を採取し，培養増殖させた後，コラーゲン・ゲル内に包埋し，軟骨変性部に移植する。コラーゲン・ゲルの表面は，本人の脛骨骨膜を採取し被覆する。術後34週で，関節鏡で確認できた症例では，正常軟骨よりやや軟らかいが，一部に硝子軟骨による再生が観察できた[10]（図10）。しかし，現在，軟骨再生医療の評価は臨床症状の改善で行われており，今後，軟骨の再生医療が実施された場合，再生軟骨のマトリクス成分の評価，強度の検定など，MRIその他の客観的，非侵襲的評価が是非必要であると考える。

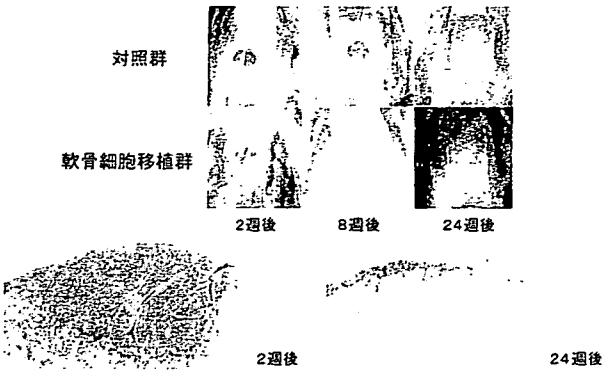

図9　ウサギ関節軟骨全層欠損に対する軟骨細胞移植術（上：肉眼的所見，下：組織学的所見）

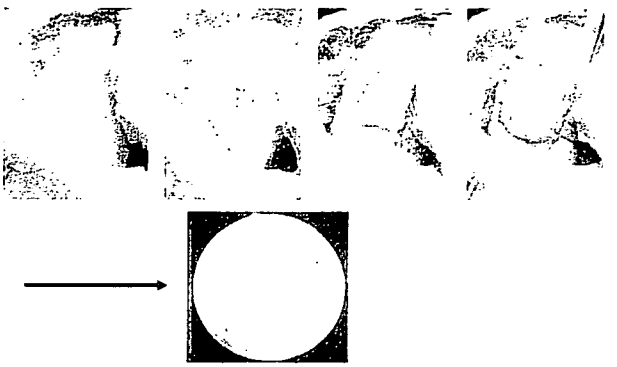

図10　変形性膝関節症に対する自家骨髄間葉系細胞移植術（上：軟骨細胞移植後骨膜にてシールし，縫合する，下：術後34週での関節鏡所見）

半月板の再生

半月板損傷はスポーツで多い膝外傷として知られ，痛みや膝がスムーズに動かずひっかかるなどの症状のためスポーツ活動に支障をきたす。しかし，半月板損傷の修復，再生の治療は困難で，いまだ発展途上といえる。半月板治療は，かつては半月切除術が多く行われてきたが，すでに50年以上も前にFairbanksが半月切除術ののちに膝の障害をきたし変形性関節症にいたることを報告し，それ以後も半月切除による問題点が多く指摘されている[11]。近年では半月縫合術をはじめとする修復治療が行われるようになり，関節鏡技術の進歩とともに適応もひろがりつつあるが，なお限界もあり，半月板の修復，再生の治療は困難である。半月板の研究のスタートは，実験動物のウサギを用いて細胞や器官培養実験から半月細胞はfibrochondrocyteと呼ばれる独特の細胞であると報告されたのに続き[12]，ヒト半月で生化学的な研究が行なわれ[13]，さらに近年では，ブタ半月で成長因子や力学的刺激による影響が調べられている[14]。最近では，半月移植用に組織やscaffoldを用いた半月の再生の研究が行われている[15][16]（図11）。我々は，ヒト半月細胞の抽出，初代培養，scaffoldを用いた3次元培養，半月細胞と骨髄由来間葉系細胞を用いた力学刺激による半月再生を試みている。現在，ミニブタを用いて，半月損傷の実験モデルを作成し，半月板細胞とコラーゲンscaffoldを用いた移植用

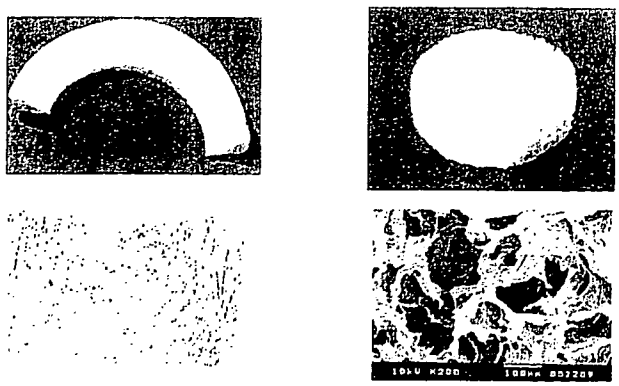

図11 半月板再生のためのコラーゲンScaffold（左：ReGen Biologics社製，右：高研社製）

培養半月にて半月再生実験を行っている。この動物実験モデルにて，修復不能な半月損傷が自家半月細胞を含むコラーゲンscaffoldにて補填した場合には修復像がみられ，半月再生に有効であると考えられ，解析を進めている。

おわりに

骨・軟骨・半月板の再生医学の現状と今後の臨床応用の可能性について述べた。骨という力学的強度を必要とする組織再生には，NEOBONEのような優れた生体材料の開発が必須である。また，その特長である連通気孔構造を生かしてBMPなどの分化／増殖因子や骨形成性細胞を気孔内に導入した生体活性型の人工骨開発への応用が期待される。軟骨の再生については，骨と比べ，未だ臨床応用が遅れているのが現状であり，より優れた担体と細胞導入法の開発が今後も必要である。BMPなどの分化／増殖因子を併用した新しい治療法の開発も必要であると考える。半月板の再生には，半月板細胞とコラーゲンscaffoldを用いた半月が最も期待されるが，再生半月の耐久性など今後検討すべき課題が多いのが現状である。今後，組織工学，分子生物学の進歩により，新しい担体，活性促進薬の開発がなされ，骨・軟骨・半月板の再生医療がさらに発展することを期待する。

文　献

1) Uchida A, Araki N, *et al.*: The use of calcium hydroxyapatite ceramic in bone tumor surgery. J Bone Joint Surg 72-B: 298-302, 1990.
2) Yoshikawa H, Uchida A: Clinical application of calcium hydroxyapatite ceramic in bone tumor surgery. Handbook of Biomaterials Engineering. Wise DL, (ed), Marcel Dekker Inc., 1999, pp433-455.
3) Tamai N, Myoui A, *et al.*: Novel hydroxyapatite ceramics with an interconnective porous structure exhibit superior osteoconduction in vivo. J Biomed Mater Res 59: 110-117, 2002.
4) Nishikawa M, Myoui A, *et al.*: Bone tissue engineering using novel interconnected porous hydroxyapatite ceramics combined with marrow mesenchymal cells: Quantitative and three-dimensional image analysis. Cell Transplantation 13: 367-376, 2004.
5) Akita S, Tamai N, *et al.*: Capillary vessel network integration by inserting a vascular pedicle enhances bone formation in tissue-engineered bone using interconnected porous hydroxyapatite ceramics. Tissue Engineering 10: 789-795, 2004.
6) Kaito T, Myoui A, *et al.*: Potentiation of the activity of bone morphogenetic protein-2 in bone regeneration by a PLA-PEG/hydroxyapatite composite. Biomaterials 26: 73-79, 2005.
7) Matsusue Y, Kotake T, *et al.*: Arthroscopic osteochondral autograft transplantation for chondral lesion of the tibial plateau of the knee. Arthroscopy 17: 653-659, 2001.
8) Minas T, Nehrer S: Current concepts in the treatment of articular cartilage defects. Orthopedics 20: 525-538, 1997.
9) Wakitani S, Goto T, *et al*: Mesenchymal cell-based repair of large full- thickness defects of articular cartilage. J Bone Joint Surg 76A: 579-592, 1994.
10) Wakitani S, Imoto K, *et al.*: Human autologous culture expanded bone marrow mesenchymal cell transplantation for repair of cartilage defects in osteoarthritic knees. Osteoarthritis Cartilage 10: 199-206, 2002.
11) Fairbank TJ: Knee joint changes after meniscectomy. J Bone Joint Surg 30B: 664-670, 1948.
12) Collier S, Ghosh P: Effects of transforming growth factor beta on proteoglycan synthesis by cell and explant cultures derived from the knee joint meniscus. Osteoarthritis Cartilage 3: 127-138, 1995.
13) Tanaka T, Fujii K, *et al.*: Comparison of biochemical characteristics of cultured fibrochondrocytes isolated from the inner and outer regions of human meniscus. Knee Surg Sports Traumatol Arthrosc 7: 75-80, 1999.
14) Lietman SA, Hobbs W, *et al.*: Effects of selected growth factors on porcine meniscus in chemically defined medium. Orthopedics 26: 799-803, 2003.
15) Rodkey WG, Steadman JR, *et al.*: A clinical study of collagen meniscus implants to restore the injured meniscus. Clin Orthop 367: S281-292, 1999.
16) Mueller SM, Shortkroff S, *et al.*: Meniscus cells seeded in type I and type II collagen-GAG matrices in vitro. Biomaterials 20: 701-709, 1999.

Available online at www.sciencedirect.com
SCIENCE DIRECT
Biomaterials 26 (2005) 73–79
Biomaterials
www.elsevier.com/locate/biomaterials

Potentiation of the activity of bone morphogenetic protein-2 in bone regeneration by a PLA–PEG/hydroxyapatite composite

Takashi Kaito[a,*], Akira Myoui[a], Kunio Takaoka[b], Naoto Saito[c], Masataka Nishikawa[a], Noriyuki Tamai[a], Hajime Ohgushi[d], Hideki Yoshikawa[a]

[a] *Department of Orthopaedic Surgery, Osaka University Graduate School of Medicine, 2-2 Yamadaoka, Suita, Osaka, 565-0871, Japan*
[b] *Department of Orthopaedic Surgery, Shinshu University School of Medicine, 3-3-1 Asahi Matsumoto, Nagano 390-8621, Japan*
[c] *Department of Orthopaedic Surgery, Osaka City University Graduate School of Medicine, 1-5-7 Asahimachi, Abeno-ku, Osaka 545-0051, Japan*
[d] *Tissue Engineering Research Center (TERC), National Institute of Advanced Industrial Science and Technology (AIST), 3-11-46, Nakoji, Amagasaki, Hyogo 661-0974, Japan*

Received 14 December 2003; accepted 3 February 2004

Abstract

Bone morphogenetic proteins (BMPs) are biologically active molecules capable of inducing new bone formation, and show potential for clinical use in bone defect repair. However, an ideal system for delivering BMPs that can potentiate their bone-inducing ability and provide initial mechanical strength and scaffold for bone ingrowth has not yet been developed. In this study, to construct a carrier/scaffold system for BMPs, we combined two biomaterials: interconnected-porous calcium hydroxyapatite ceramics (IP-CHA), and the synthetic biodegradable polymer poly D,L,-lactic acid–polyethyleneglycol block co-polymer (PLA–PEG). We used a rabbit radii model to evaluate the bone-regenerating efficacy of rhBMP-2/PLA–PEG/IP-CHA composite. At 8 weeks after implantation, all bone defects in groups treated with 5 or 20 μg of BMP were completely repaired with sufficient strength. Furthermore, using this carrier scaffold system, we reduced the amount of BMP necessary for such results to about a tenth of the amount needed in previous studies, probably due to the superior osteoconduction ability of IP-CHA and the optimal drug delivery system provided by PLA–PEG, inducing new bone formation in the interconnected pores. The present findings indicate that the synthetic biodegradable polymer/IP-CHA composite is an excellent combination carrier/scaffold delivery system for rhBMP-2, and that it strongly promotes the clinical effects of rhBMP-2 in bone tissue regeneration.

Keywords: BMP (bone morphogenetic protein); Hydroxyapatite; Drug delivery; Polylactic acid; Bone tissue engineering

1. Introduction

Bone defects due to tumor resection, trauma and congenital abnormality are a great challenge to reconstructive surgery. Autologous bone grafting is a popular procedure, but it has many disadvantages such as limited supply of suitable bone and persistence of pain, nerve damage, fracture and cosmetic disability at the donor site. There are no donor site problems with allografting, but it involves risks of disease transmission and immunological reaction [1]. For these reasons, it is hoped that treatment with bone morphogenetic proteins (BMPs), which belong to the transforming growth factor (TGF) superfamily and are known to be capable of eliciting new bone formation both orthotopically and heterotopically in experimental animal models, can provide an alternative to bone grafting [2–4]. Three types of BMP-based bone tissue engineering have been tried to date: cell therapy, gene therapy, and cytokine therapy. Cell therapy involves transplantation of autogenous bone marrow mesenchymal cells differentiated by BMP. Gene therapy involves transduction of genes encoding BMPs into cells at the repair site. Cytokine therapy involves recombinant BMP and carriers that retain and release BMP as needed. Cytokine therapy is considered the most promising of these approaches for practical use [5].

In cytokine therapy, the drug delivery system should not only promote effective biological activity but also limit spatial spread of the cytokine as appropriate [6].

*Corresponding author. Tel.: +81-06-6879-3552; fax: +81-06-6879-3559.
E-mail address: t-kaito@leto.eonet.ne.jp (T. Kaito).

0142-9612/$ - see front matter © 2004 Elsevier Ltd. All rights reserved.
doi:10.1016/j.biomaterials.2004.02.010

Many materials have been evaluated as carriers for BMP, including synthesized polymer, collagen, tricalcium phosphate, and classical hydroxyapatite. Although all of these materials can induce bone formation in ectopic and orthotopic sites, they have not yet gained widespread use because of disadvantages such as risk of disease transmission, fragility, difficulty in handling, lack of porous structures suitable for cell infiltration, and limited supply [7–11].

Another important unresolved issue in BMP-based bone regeneration is the amount of BMP necessary to induce sufficient new bone formation in humans. For example, due to differences in responsiveness to BMP, humans respond to quantities in mg to induce new bone formation, whereas mice, BMP quantities in μg is sufficient [12,13].

To resolve these issues, the present delivery system combines two biomaterials: a three-dimensional interconnected porous scaffold with initial mechanical strength and bone conduction ability, and a biodegradable synthetic polymer that provides sustained release of BMP. The scaffold we chose was a fully interconnected porous calcium hydroxyapatite ceramic (IP-CHA) that we developed using a "foam-gel" technique. Previously, we showed that IP-CHA has superior osteoconduction ability [14]. The carrier we selected was poly D,L-lactic acid–polyethylene glycol block copolymer (PLA–PEG), which is reportedly an effective carrier material for recombinant human BMP-2 (rhBMP-2) [15,16].

This report describes the bone-inducing effects of a PLA–PEG/IP-CHA composite containing a small amount of rhBMP-2, in a rabbit radius segmental defect model.

2. Materials and methods

2.1. Preparation of implants

Cylindrical pieces of IP-CHA (diameter, 4 mm; height, 15 mm) were provided by Toshiba Ceramics Co., Ltd (Kanagawa, Japan). IP-CHA has a well-organized interconnected structure with total porosity of 75% and average interconnection channel diameter of 40 μm. Theoretically, more than 90% of the pores are connected to channels with a diameter greater than 10 μm, allowing tissue invasion from pore-to-pore [14].

The rhBMP-2, which was produced at the Genetics Institute (Cambridge, MA) and donated to us through Yamamouch Pharmaceutical Co., Ltd. (Ibaraki, Japan), was dissolved in a buffer (5 mM glutamic acid, 2.5% glycine, 0.5% sucrose, and 0.01% Tween 80) at a concentration of 1 μg/μl.

PLA-PEG with a total molecular weight of 11 400 Da and a PLA:PEG molar ratio of 51:49 was synthesized and provided by Taki Chemicals Co., Ltd (Hyogo, Japan).

The polymer mass was liquidized in acetone and mixed with 5 or 20 μg of rhBMP-2. Next, this mixture was dropped onto the IP-CHA (Fig. 1A), and the acetone was then removed by evaporation in a safety cabinet to return the polymer to its native state.

2.2. Scanning electron microscopy (SEM)

To verify that the pore surface of IP-CHA was coated by rhBMP-2/PLA-PEG homogenously, the implants were cut into halves across the longitudinal axis and the cut surface was observed with a scanning electron microscope (JSM-6000F, Nihon Denshi Oyo Co., Ltd., Tokyo, Japan).

2.3. Animal experiment

Thirty New Zealand white rabbits weighing an average of 3.5 kg were used. The animals were anesthetized using an intra-venous injection of 50 mg pentobarbital and 25 mg xylazine hydrochloride, together with a subcutaneous injection of 0.5 ml of 1% lidocaine with 0.01% epinephrine around the operative site. An approximately 3-cm-long incision was made, and the tissues overlying the distal diaphyseal radius were dissected. A 1.5-cm segmental osteoperiosteal defect was created in the radius with a mini-oscillating saw. Ten animals each were implanted with rhBMP-2/–PLA–

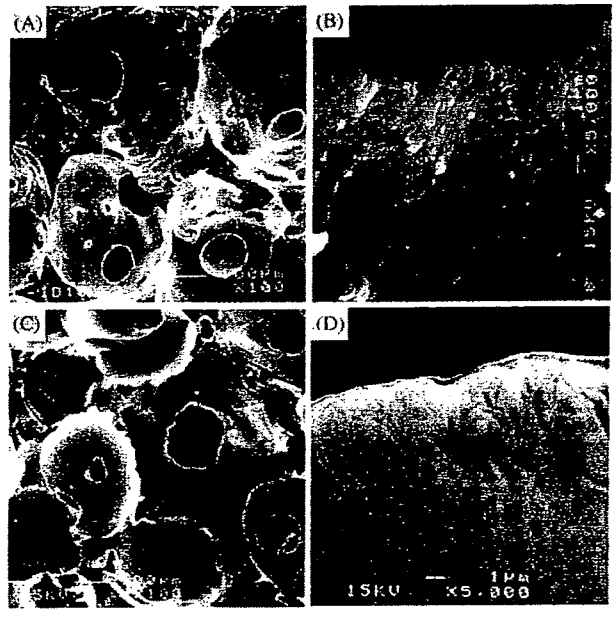

Fig. 1. SEM photographs of IP-CHA before (A,B) and after (C,D) PLA–PEG coating. Magnification: (A,C) × 100; (B,D) × 5000. (A) Large spherical pores (diameter, 100–200 μm) were divided by thin walls and interconnected to one another. (B) Before PLA–PEG coating, individual hydroxyapatite particles were clearly visible. (C) After coating, at lower magnification, interconnecting channels were still clearly visible. (D) At higher magnification, the boundaries between individual hydroxyapatite particles became ambiguous.

PEG/IP-CHA composite containing 5 μg (5 μg BMP group) or 20 μg (20 μg BMP group) of rhBMP-2. These two groups were each subdivided into two subgroups ($n=5$), which were sacrificed at 4 and 8 weeks after implantation, respectively. In five animals (defect group), nothing was implanted in the defect; these animals were sacrificed at 8 weeks. In five animals (IP-CHA alone group), IP-CHA without BMP/PLA–PEG coating was implanted; these animals were sacrificed at 8 weeks. Animals were kept in the Institute of Experimental Animal Sciences (IEXAS), Osaka University Medical School, in accordance with the institutional guidelines for care and use of laboratory animals. Sacrifice was performed by overdose anesthesia, and implanted forearms were harvested together with surrounding tissues.

2.4. Radiographic examination and bone mineral density (BMD)

All harvested tissues were fixed with 10% neutral formalin and then radiographed with a soft X-ray apparatus (MX-20 Faxitron, Torrex and Micro Focus Systems, Wheeling, IL). BMD was determined by dual-energy X-ray absorptiometry (DXA) using an animal densitometer (PIXImus, Lunar Corp., Madison, WI). In scans of the excised bones, the region-of interest (ROI) was positioned over the whole implant area (IP-CHA) on the anterior–posterior view, not including host bone or bone that developed outside the implant. BMD was determined using the image analysis software provided with the instrument.

2.5. Microfocus-computed tomography (CT) and mechanical evaluation

From four animals in each group, two 4-mm-high discs were carved from the center of the cylindrical IP-CHA blocks: one for CT and histological evaluation, and the other for mechanical evaluation. Bone formation in IP-CHA pores was evaluated using a microfocus CT system (MCT-CB100MF(Z); Hitachi Medical Corporation, Tokyo, Japan). After fixation in 10%-buffered formalin, each sample was scanned at intervals of 10 μm, at 50 kV and 200 μA. Analytical conditions were super-precision mode and 7-times magnification, with an image intensifier field of 1.8 in. The radiodensity of the newly formed bone on CT images was determined by comparing the histological section with the corresponding CT image. Then, the newly formed bone area on the CT images was extracted, and its volume was measured using the software package TRI3D-BON (Ratoc System Engineering Co., Ltd., Tokyo, Japan). Compression tests were performed using AUTOGRAPH AG-10KNI (Shimadzu Corp., Kyoto, Japan), with a compression speed of 1 mm/min. Testing was performed vertically towards the specimen, along the longitudinal axis of the radius.

2.6. Histological evaluation

One of the five tissue samples from each group was demineralized with 50% formic acid and 10% sodium citrate, dehydrated through an ethanol series and embedded in paraffin wax. Sections (thickness, 5 μm) were cut, stained with hematoxylin and eosin, and examined under a light microscope.

2.7. Statistical analysis

BMD, compressive strength, and bone volume were compared between IP-CHA, BMP 5 μg and BMP 20 μg groups using ANOVA, followed by Turkey–Kramer test post test. A P value of <0.05 was considered to indicate statistical significance.

3. Results

3.1. Scanning electron microscopy

After PLA–PEG coating, pore surface and interconnecting channels of the composite were surveyed with a SEM at ×100 (Fig. 1A,C) and ×5000 (Fig. 1B,D) magnification. In original IP-CHA, at ×5000 magnification, boundaries of individual hydroxyapatite particles were clearly visible (Fig. 1B). After PLA–PEG coating, the boundaries became ambiguous, suggesting that the thin PLA–PEG layer covered the entire surface of the pores (Fig. 1D). At ×100 magnification, interconnecting channels were still clearly visible after PLA–PEG coating (Fig. 1A,C).

3.2. Radiographic evaluation

In the defect group, although a minimal amount of new bone was observed at both ends of the defect at 8 weeks, the defect was not repaired, indicating that the defect size was critical in this model. Similarly, in the IP-CHA alone group, small areas at both ends of the implant were radiopaque at 8 weeks, but radiolucent lines were clearly visible between the implant and host bone, suggesting non-union. In contrast, in both 5 μg and 20 μg BMP groups, the entire implant was highly radiopaque at 4 weeks after implantation. In the 5 μg BMP group, a small amount of radiopaque shadow was observed outside the implant, mainly at the junctional sites. In the 20 μg BMP group, a radiopaque shadow up to 2 mm thick covered nearly the entire implant. Eight weeks after implantation, in both BMP 5 and 20 μg groups, the radiodensity of the implants had further increased, and excess newly formed bone outside the

implants had been remodeled to form a smooth repair (Fig. 2). Table 1 summarizes the results of radiographic evaluation. In both BMP groups, all implants showed bilateral union and sclerotic change of the entire implant by 4 weeks after surgery. However, in the IP-CHA alone group, only two implants exhibited unilateral union and none showed sclerotic change (Table 1).

3.3. Histology

Macroscopic appearance of the histological sections was consistent with the findings of radiographic examination. In both BMP groups, at 4 weeks after implantation, almost all pores in the IP-CHA were filled with trabecular bone and hematopoietic marrow. The junctions between the implant and host bone were bony fused, involving new bone formation outside the implant and in the marrow cavity of the bone adjacent to the implant. In the 20 μg BMP group, prominent bone formation covering almost the entire implant was observed. The newly formed bone observed at 4 weeks outside the implant and in the marrow cavity had disappeared at 8 weeks, suggesting resorption of excess new bone in remodeling. Interestingly, pores in the outer part of the cylindrical implant were filled predominantly by dense bone matrix like cortical bone, and pores in the central part contained abundant hematopoietic marrow. In contrast, in the IP-CHA group, little bone tissue was found in the pores at both ends of the implants, and most pores were filled with fibrous tissue at 8 weeks after implantation (Fig. 3).

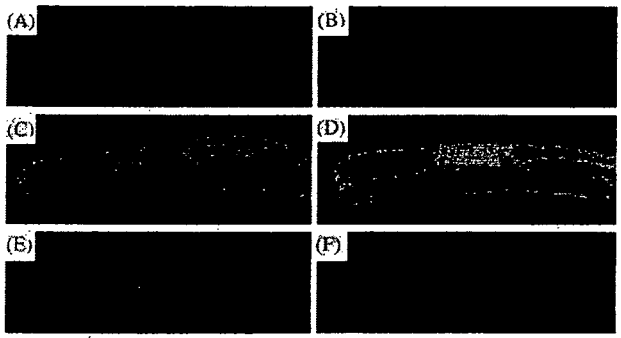

Fig. 2. Soft X-ray photographs. Defect group at 8 weeks after operation (A). IP-CHA alone group at 8 weeks after implantation (B). BMP 5 μg group: at 4 weeks (C) and 8 weeks (D). BMP 20 μg group: at 4 weeks (E) and 8 weeks (F). In IP-CHA alone group, radiolucent lines were clearly visible between the implant and host bone, and the radiodensity of the implant had not increased at 8 weeks (B). In the 5 and 20 μg BMP groups, radiopaque shadows were observed at junctional sites, the entire implant was radiopaque at 4 weeks (C,E), and the radiodensity had further increased at 8 weeks (D,F).

3.4. BMD

In both BMP groups, BMD had increased significantly at 4 weeks after implantation. At 4 weeks, the 20 μg BMP group had a higher mean BMD than the BMP 5 μg group. However at 8 weeks after implantation, probably due to remodeling (as indicated by soft X-ray and histology), the BMP 5 and 20 μg groups had

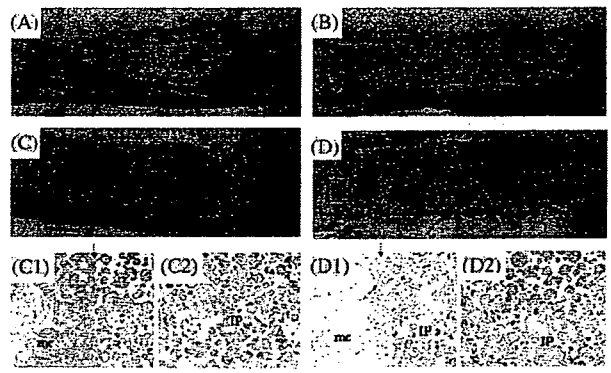

Fig. 3. Low-power photomicrographs of defects: without treatment, at 8 weeks after surgery (A); treated with IP-CHA alone, at 8 weeks (B); BMP 5 μg group, at 4 weeks (C) and at 8 weeks (D). High-power photomicrographs of 5 μg BMP group at 4 weeks (C1,C2) and 8 weeks (D1,D2) after surgery. At 4 weeks after surgery, almost all pores in the IP-CHA were evenly filled with trabecular bone and hematopoietic marrow (C2), and newly formed bone was found in the marrow cavity of host bone (C1). At 8 weeks after surgery, an interesting pattern was observed. Pores in the outer part of the cylindrical implant were filled with dense bone matrix, and pores in the center were filled with abundant hematopoietic marrow (D2). Newly formed bone in the marrow cavity was absorbed (D1). mc, marrow cavity; IC, IP-CHA. Arrows indicate implant end (magnification: × 40).

Table 1
Summary of radiographic evaluation

Groups	4 weeks		8 weeks	
	Gain of opacity[a]	Junction with bony union[b](union/junction)	Gain of opacity	Junction with bony union(union/junction)
IP-CHA alone			0/5	2/10
BMP 5 μg	5/5	10/10	5/5	10/10
BMP 20 μg	5/5	10/10	5/5	10/10

[a] Number of implants that gained radiopacity.
[b] Each implants has two junctions between host bone. These data shows union junction per total junctions (10).

almost the same mean BMD, which was about twice as high as that of the IP-CHA group (Fig. 4).

3.5. Mechanical compression test

The initial breaking load of IP-CHA was approximately 100 N. In the IP-CHA alone group, breaking load did not increase until 8 weeks after implantation. In contrast, in both BMP groups, breaking load steadily increased until 8 weeks after implantation, and the final strength was as high as about 800 N. In both BMP groups, at 4 and 8 weeks after implantation, breaking load was significantly greater than the initial value. There was no significant difference between the BMP groups (Fig. 5).

3.6. Microfocus-CT evaluation

In both BMP groups, mineralized bone matrix newly formed in the porous area of the ceramics was detectable by microfocus CT at 4 weeks after implantation, and the bone volume in the pores was maintained until 8 weeks after implantation. At 8 weeks, in both BMP groups, bone volume was significantly greater than in the IP-CHA alone group. There was no significant difference in bone volume in the pores between the BMP groups (Fig. 6).

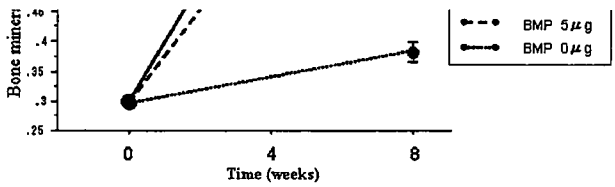

Fig. 4. Bone mineral density of IP-CHA alone group and BMP 5 and 20 μg groups was evaluated by dual-energy X-ray absorptiometry (DXA) using a PIXImus animal densitometer. Each data point represents an average and standard deviation ($n=5$).

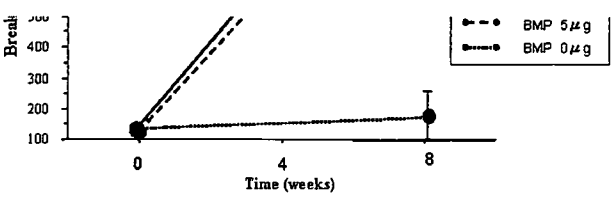

Fig. 5. Breaking load of IP-CHA alone group and BMP 5 and 20 μg groups in compression strength test. Each data point represents an average and standard deviation ($n=4$).

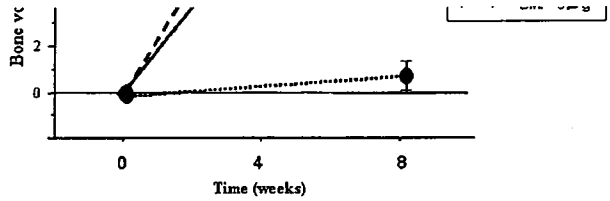

Fig. 6. Bone volume in the pore area of IP-CHA was evaluated using the software package TRI3D-BON (Ratoc System Engineering Co., Ltd., Tokyo, Japan) and the sectional data of the micro-CT image. Each data point represents an average and standard deviation ($n=4$).

4. Discussion

The present findings demonstrate that a PLA–PEG/IP-CHA composite containing 5 or 20 μg of rhBMP-2 can induce new bone formation in pores and around the implant, leading to complete repair of a critical-size bone defect in rabbit radius with sufficient strength and anatomical structure. Composite containing 5 μg of rhBMP-2 achieved radiographic and histological union at the junctional sites, and the implant gained radiodensity and sufficient mechanical strength. There was a dose–response relationship of rhBMP-2 at 4 weeks after implantation: the higher dose produced superior bone formation around the implant, compared to the lower dose. However, at 8 weeks after surgery, the 5 and 20 μg BMP groups had almost identical radiographic, histological and biomechanical findings. Biomechanically, breaking load of the implant at 8 weeks after surgery was about 800 N, which is almost equal to that of rabbit radius. These findings suggest that PLA–PEG/IP-CHA composite containing 5 μg of rhBMP-2 is sufficient to repair a defect of this size. This dose of BMP is about a tenth of the dose commonly used in previous reports [17–19].

The two biomaterials we combined possess several features that may contribute to the superior ability of the present composite in repair of critical-size segmental bone defects. The interconnected highly porous structure of IP-CHA, with interconnections averaging 40 μm

in diameter, allows efficient migration of bone-producing cells from pore to pore as well as invasion by vascular vessels that is essential for new bone formation. Because IP-CHA combines high porosity and high strength, its three-dimensional structure is preserved whole throughout the repair process, offering an excellent scaffold for bone ingrowth, which apparently facilitates excellent repair of size, shape and mechanical strength. The polymer (PLA–PEG) used in this study is biocompatible and biodegradable, with little inflammatory potential; thus, it does not interfere with new bone formation in the pores. When BMP/PLA–PEG is put in water or implanted in vivo, it absorbs water to form a hydrogel, and then degrades gradually and steadily. During this degradation process, BMP is released from the polymer steadily for about 3 weeks. Obviously, the lack of bony repair in the IP-CHA alone group demonstrates the importance of BMP in the repair process, but there is also another factor that seems to be important. Poly D,L-lactic acid–para dioxanone–polyethyleneglycol block co-polymer (PLA–DX–PEG) is reportedly an excellent carrier for rhBMP-2 in a mouse model of ectopic bone formation [5,20]. PLA–DX–PEG, when put in water, releases rhBMP-2 for about 2 weeks. However, in combination with IP-CHA, PLA–DX–PEG/rhBMP-2 composite induces much less bone ingrowth than PLA–PEG/rhBMP-2, which releases BMP-2 for about 3 weeks (data not shown). These findings suggest that the compatibility between scaffolding and BMP-releasing properties of this polymer is another important factor. The optimal combination may vary with factors including implant size, species and local conditions. In addition, swelling of PLA–PEG after absorption of tissue fluid may stabilize the implant and help bone-producing cells to migrate into the implant by filling the gaps between host bone and implant [5,18].

5. Conclusion

This study demonstrated that the composite of PLA–PEG synthetic co-polymer and interconnected porous hydroxyapatite containing only 5 μg of rhBMP-2 completely repaired a critical-size bone defect in rabbit radius with sufficient strength and anatomical structure. Our findings suggest that the combination of these biomaterials potentiates the activity of rhBMP-2 in bone regeneration, leading to a marked reduction of the required amount of rhBMP-2 compared with previous reports.

Acknowledgements

We thank Genetic Institute, Yamanouchi Pharmaceutical Co., Ltd., Taki Chemicals Co., Ltd., and Toshiba Ceramics Co., Ltd., for kindly providing the chemicals and other materials. We also thank Kaori Asai and Mina Okamoto for their expert technical assistance. This work was supported in part by Grants from the Ministry of Health, Labor and Welfare and Ministry of Education, Culture, Sports, Science and Technology, Japan.

References

[1] Goldberg VM. Natural history of autografts and allografts. In: Older J, editor. Bone implant grafting. London: Springer; 1992. p. 9–12.
[2] Wozney JM, Rosen V, Celeste AJ, Mitsick LM, Whitters MJ, Kriz RW, Hewick RM, Wang EA. Novel regulators of bone formation: molecular clones and activities. Science 1988;242:1528–33.
[3] Wang EA, Rosen V, D'Alessandro JS, Baudny M, Cordes P, Harada T, Israel DI, Hewick RM, Kerns KM, LaPan P, Luxenberg DP, McQuaid D, Moutsatsos IK, Nove J, Wozeny EA. Recombinant human bone morphogenetic protein induces bone formation. Proc Natl Acad Sci USA 1990;87:2220–4.
[4] Urist MR. Bone formation by autoinduction. Science 1965; 150:893–9.
[5] Saito N, Takaoka K. New synthetic biodegradable polymers as BMP carriers for bone tissue engineering. Biomaterials 2003; 24:2287–93.
[6] Miyamoto S, Takaoka K, Okada T, Yoshikawa H, Hashimoto J, Suzuki S, Ono K. Evaluation of polylactic acid homopolymers as carriers for bone morphogenetic protein. Clin Orthop 1992;278:274–85.
[7] Takaoka K, Koezuka M, Nakahara H. Telopeptide-depleted bovine skin collagen as a carrier for bone morphogenetic protein. J Orthop Res 1991;9(6):902–7.
[8] Petite H, Viateau V, Bensaid W, Meunier A, Pollak C, Bourguignon M, Oudina K, Sedel L, Guillemin G. Tissue-engineered bone regeneration. Nat Biotechnol 2000;18:959–63.
[9] Urist MR, Lietze A, Dawson E. β-tricalcium phosphate delivery system for bone morphogenetic protein. Clin Orthop 1984; 187:277–80.
[10] Miyamoto S, Takaoka K, Okada T, Yoshikawa H, Hashimoto J, Suzuki S, Ono K. Polylactic acid–polyethylene glycol block copolymer: a new biodegradable synthetic carrier for bone morphogenetic protein. Clin Orithop 1993;294:333–43.
[11] Takaoka K, Nakahara H, Yoshikawa H, Masuhara K, Tsuda T, Ono K. Ectopic bone induction on and in porous hydroxyapatite combined with collagen and bone morphogenetic protein. Clin Orthop 1988;234:250–4.
[12] Aspenberg P, Lohmander S, Thorngren KG. Monkey bone matrix induces bone formation in the athymic rats, but not in adult monkeys. J Orthop Res 1991;9:20–5.
[13] Miyamoto S, Takaoka K, Ono K. Bone induction in monkeys by bone morphogenetic protein. A trans-filter technique. J Bone Joint Surg 1993;75B:107–10.
[14] Tamai N, Myoui A, Tomita T, Nakase T, Tanaka J, Ochi T, Yoshikawa H. Novel Hydroxyapatite ceramics with an interconnective porpus structure exhibit superior osteoconduction in vivo. J Biomed Mater Res 2002;59(1):110–7.
[15] Saito N, Okada T, Horiuchi H, Murakami N, Takahashi J, Nawata M, Ota H, Nozaki K, Takaoka K. A biodegradable polymer as a cytokine delivery system for inducing bone formation. Nat Biotechnol 2001;19(4):332–5.
[16] Saito N, Okada T, Horiuchi H, Murakami N, Takahashi J, Nawata M, Ota H, Miyamoto S, Nozaki K, Takaoka K. Biodegradable poly D,L-lactic acid–polyethylene glycol block copolymers as a BMP delivery system for inducing bone. J Bone Joint Surg 2001;83-A (Suppl 1)(Part 2):S92–8.

[17] Kokubo S, Fujimoto R, Yokota S, Fukushima S, Nozaki K, Takahashi K, Miyata K. Bone regeneration by recombinant human bone morphogenetic protein-2 and a novel biodegradable carrier in a rabbit ulnar defect model. Biomaterials 2003; 24:1643–51.

[18] Murakami N, Saito N, Horiuchi H, Okada T, Nozaki K, Takaoka K. Repair of segmental defects in rabbit fumeri with titanium fiber mesh cylinders containing recombinant human bone morphogenetic protein-2 (RHBMP-2) and a synthetic polymer. J Biomed Mater Res 2002;62:169–74.

[19] Wheeler DL, Chamberland DL, Schimitt JM, Buck DC, Brekke JH, Hollinger JO, Joh SP, Suh KW. Radiomorphometry and biomechanical assessment of recombinant human bone morphogenetic protein 2 and polymer in rabbit radius ostectomy model. J Biomed Mater Res 1998;43(4):365–73.

[20] Murakami N, Saito N, Takahashi J, Ota H, Horiuchi H, Nawata M, Okada T, Nozaki K, Takaoka K. Repair of a proximal femoral bone defect in dogs using a porous surfaced prosthesis in combination with recombinant BMP-2 and synthetic polymer carrier. Biomaterials 2003;24:2153–9.

ELSEVIER

Bone 37 (2005) 607 – 621

BONE

www.elsevier.com/locate/bone

Leptin regulates chondrocyte differentiation and matrix maturation during endochondral ossification

Yuki Kishida[a], Makoto Hirao[a], Noriyuki Tamai[a], Akihide Nampei[a], Tetsuho Fujimoto[a], Takanobu Nakase[b], Nobuyuki Shimizu[a], Hideki Yoshikawa[a], Akira Myoui[a,*]

[a]*Department of Orthopaedic Surgery, Osaka University Graduate School of Medicine, 2-2 Yamadaoka, Suita, Osaka 565-0871, Japan*
[b]*Department of Orthopaedic Surgery, Osaka National Hospital, Japan*

Received 12 January 2005; revised 6 May 2005; accepted 24 May 2005
Available online 20 July 2005

Abstract

Leptin has been suggested to mediate a variety of actions, including bone development, via its ubiquitously expressed receptor (Ob-Rb). In this study, we investigated the role of leptin in endochondral ossification at the growth plate. The growth plates of wild-type and ob/ob mice were analyzed. Effects of leptin on chondrocyte gene expression, cell cycle, apoptosis and matrix mineralization were assessed using primary chondrocyte culture and the ATDC5 cell differentiation culture system. Immunohistochemistry and in situ hybridization showed that leptin was localized in prehypertrophic chondrocytes in normal mice and that Ob-Rb was localized in hypertrophic chondrocytes in normal and ob/ob mice. Growth plates of ob/ob mice were more fragile than those of wild-type mice in a mechanical test and were broken easily at the chondro-osseous junction. The growth plates of ob/ob mice showed disturbed columnar structure, decreased type X collagen expression, less organized collagen fibril arrangement, increased apoptosis and premature mineralization. Leptin administration in ob/ob mice led to an increase in femoral and humeral lengths and decrease in the proportional length of the calcified hypertrophic zone to the whole hypertrophic zone. In primary chondrocyte culture, the matrix mineralization in ob/ob chondrocytes was stronger than that of wild-type mice; this mineralization in both types of mice was abolished by the addition of exogenous leptin (10 ng/ml). During ATDC5 cell differentiation culture, exogenous leptin at a concentration of 1–10 ng/ml (equivalent to the normal serum concentration of leptin) altered type X collagen mRNA expression and suppressed apoptosis, cell growth and matrix calcification. In conclusion, we demonstrated that leptin modulates several events associated with terminal differentiation of chondrocytes. Our finding that the growth plates of ob/ob mice were fragile implies a disturbance in the differentiation/maturation process of growth plates due to depletion of leptin signaling in ob/ob mice. These findings suggest that peripheral leptin signaling plays an essential role in endochondral ossification at the growth plate.

Keywords: Leptin; Growth plate; Endochondral ossification; ob/ob mouse; Bone chondrocyte differentiation

Introduction

Leptin, a 16-kDa protein encoded by the obese (ob) gene, hormonally regulates food intake and energy expenditure by negative feedback at the hypothalamic nuclei [1]. Leptin is expressed predominantly in adipose tissue of normal mice and is absent in ob/ob mice, which are homozygous for the ob mutation. Leptin is thought to act primarily at the hypothalamus, where it has effects on appetite, energy expenditure and neuroendocrine axes [2].

Recent studies show that leptin is produced in placenta, skeletal muscle, fetal bone/cartilage and primary cultures of human osteoblasts [3–6]. In addition to its effects on the central nervous system, leptin reportedly exerts effects on cells in peripheral tissues via high-affinity leptin receptors [3–9].

Several reports show that leptin deficiency in humans and mice leads to phenotypic abnormalities in skeletal development, the endocrine system, the immune system and the sympathetic nervous system [10–12]. A human with

* Corresponding author. Fax: +81 6 6879 3559.
E-mail address: myoi@ort.med.osaka-u.ac.jp (A. Myoui).

8756-3282/$ - see front matter © 2005 Elsevier Inc. All rights reserved.
doi:10.1016/j.bone.2005.05.009

congenital leptin deficiency reportedly exhibited advanced bone age, indicating abnormalities in bone development [13]. Femora of ob/ob mice are shorter than those of wild-type mice [8]. Linear growth occurs by endochondral bone formation, in which epiphyseal growth plate chondrocytes undergo an organized program of proliferation, maturation, hypertrophic conversion and calcification [14–17]. Thus, the available evidence indicates that leptin has an important function in the growth plate and plays a key role in endochondral ossification. However, there have been few studies of the role of leptin in the regulation of endochondral ossification in vitro or in vivo.

In the present study, we examined the growth plate cartilage of long bones in ob/ob mice. In addition, we analyzed the effect of leptin on chondrocytic differentiation of in vitro using primary chondrocyte culture and murine ATDC5 chondrocytic cell line. The present results suggest that leptin plays an important role in the regulation of physiological processes of endochondral ossification in growth plate cartilage.

Material and methods

Animals

Ob/ob mice were purchased from the Jackson Laboratory (Bar Harbor, ME, USA). All mice were housed under specific pathogen-free conditions with a 12-h light and dark cycle. Intercrossing of heterozygous animals produced homozygous ob/ob mice and wild-type mice. Under anesthesia, 0.5 cm of the tail of each mouse was removed, and genomic DNA was extracted from this material using a DNA mini kit (Qiagen, Valencia, CA, USA). Genotyping was performed using the method of Namae et al. [18]. The housing, care and experimental protocol were approved by the Animal Care and Use Committee of Osaka University.

Measurement of femoral and humeral length

Femora and humeri of 4-week-old wild-type ($n = 10$) and ob/ob mice ($n = 6$) were radiographed and analyzed using Scion Image software (Scion Corporation, Frederick, MD, USA) to determine femoral and humeral length.

Immunohistochemistry and histological analysis

The femora, tibiae and humeri were removed, fixed in 4% paraformaldehyde (Merck, Darmstadt, Germany) in phosphate-buffered saline (PBS, pH 7.4; Sigma, St. Louis, MO, USA), decalcified in 20% EDTA, dehydrated through an ethanol series, embedded in paraffin and then cut into 4-μm sections. Immunohistochemistry was performed using the streptavidin–peroxidase method with Histofine SAB-PO kits and an aminoethyl carbazole (AEC) substrate kit (Nichirei, Tokyo, Japan) according to the manufacturer's protocol. Tissue sections were deparaffinized, hydrated in PBS and incubated in 3% H_2O_2 in methanol for 20 min at room temperature to block endogenous peroxidase activity. After being washed in PBS, the sections were preincubated with 10% normal serum from the same species as the secondary antibody (to minimize background staining) for 20 min at room temperature. Sections were then incubated with two different primary antibodies, anti-leptin polyclonal antibody (Santa Cruz Biotechnology, Santa Cruz, CA, USA) and anti-leptin receptor polyclonal antibody (Santa Cruz Biotechnology) overnight at 4°C. After washing in PBS, the sections were incubated with secondary antibody for 20 min at room temperature. Sections were then incubated with peroxidase-conjugated streptavidin for 20 min at room temperature and washed in PBS. Finally, visualization was performed using AEC as a substrate. As a control for immunostaining, normal serum from the same species as the primary antibodies was used instead of the primary antibodies.

In situ hybridization

A 500-bp leptin fragment and a 450-bp Ob-Rb fragment were cut out and then inserted into pGEM-T easy plasmid (Promega, Madison, WI, USA). The plasmid was linearized with *Nco*I or *Spe*I. Then, in vitro transcription and digoxigenin labeling were performed to prepare sense or antisense RNA probes, respectively, using the digoxigenin RNA labeling kit (Roche Diagnostics, Lewes, UK). Paraffin-embedded sections were deparaffinized, rehydrated and heated in 100 mM citric acid buffer in a microwave oven (H2800 Microwave Processor; Energy Beam Sciences, Agawam, MA, USA) at 95°C for 10 min. Then, sections were treated with 1 μg/ml proteinase K at 37°C for 5 min and treated with 0.2 M HCl for 20 min to quench endogenous alkaline phosphatase. Each section was covered with a single-strand RNA probe and 50 μl of hybridization solution (Dako Cytomation, Kyoto, Japan) and then incubated at 50°C for overnight. After hybridization, the slides were washed at 50°C. RNaseA treatment (10 μg/ml) proceeded at 37°C for 20 min. Hybridized signals were detected by a color reaction using 4-nitroblue tetrazolium chloride and 5-bromo-4-chloro-3-indolyl phosphate (Dako).

Mechanical test

Tibiae of 8-week-old wild-type ($n = 10$) and ob/ob ($n = 6$) mice were used. The muscles were removed, and the bones were wrapped with normal saline-soaked gauze. The bones were stored in a plastic bag at −80°C before processing. The distal part of the tibia was embedded in resin (Tray Resin II; Shofu, Kyoto, Japan) and secured so that the load-bearing axis was parallel to the anterior–posterior axis of the proximal growth plate. The proximal epiphysis was loaded with 20 N at 10 mm/min using a testing machine (MZ-500D; Marto, Tokyo, Japan). The

maximum load required to break the material was determined. The bone specimens were kept wet in saline during all stages of tissue preparation. After the mechanical test, they were fixed in 10% formalin, decalcified, embedded in paraffin, cut into 4-μm sections and stained with hematoxylin and eosin (H–E).

RNA extraction and reverse transcription polymerase chain reactions (RT-PCR)

Total RNA was extracted from cells using ISOGEN reagent (Nippon Gene, Tokyo, Japan). The cDNA was synthesized using the SuperScript First-Strand Synthesis System (Invitrogen, Carlsbad, CA, USA) and was then incubated with 1 unit of *Escherichia coli* RNase H at 37°C. PCR was performed using Ready to Go PCR beads (Amersham Biosciences, Piscataway, NJ, USA). The oligonucleotide PCR primer sequences and amplification profiles used are described elsewhere [19]. The amplification reaction products were resolved on 2.0% agarose/Tris–acetate buffer gels, electrophoresed at 100 mV and visualized by ethidium-bromide staining. Real-time PCR was preformed to clarify the expression of type X collagen in growth plates of wild-type mice and ob/ob mice. The growth plates of femora and humeri of 4-week-old wild-type mice (n = 4) and ob/ob (n = 4) mice were isolated after aseptic dissection and pounded in liquid nitrogen. Total RNA was extracted from tissue and the cDNA was synthesized, as described above. Real-time PCR was performed using a LightCycler rapid thermal cycler system (Roche Diagnostics) according to the manufacturer's instructions. Reactions were performed in a 20-μl volume with 0.5 μM primers and 2.5 μM $MgCl_2$. Nucleotides, Taq DNA polymerase and buffers were included in the Light-Cycler-DNA Master SYBER Green I Mix (Roche Diagnostics). The plasmid used as the standard DNA was constructed by ligation of a type X collagen PCR product and a G3PDH fragment in pGEM-T Easy vector according to the instructions of the manufacturer (Promega). The concentrations of plasmid preparations were determined by measuring the optical density at 260 nm. The relative amount of gene transcript present was calculated and normalized by dividing the value calculated for the gene of interest by the value calculated for the housekeeping gene. These experiments were repeated three times.

Electron microscopy

Tibiae of 4-week-old wild-type (n = 4) and ob/ob mice (n = 4) were fixed in 2.5% glutaraldehyde and then in OsO_4. The specimens were dehydrated in a graded series of ethanol, embedded in epoxy resin, cut into ultrathin sections and stained with uranium acetate and lead citrate. Sections were examined using a transmission electron microscope (H-300, Hitachi, Tokyo, Japan) operated at 75 kV, and the diameter of collagen fibrils was measured.

TUNEL reaction

Terminal deoxynucleotidyl transferase-mediated dUTP nick end labeling (TUNEL) staining was performed using in situ apoptosis detection kits (TAKARA Bio, Otsu, Japan). Sections cut from paraffin-embedded specimens of the tibiae of 4-week-old (wild type: n = 5, ob/ob: n = 4) and 8-week-old mice (wild type: n = 8, ob/ob: n = 4) were deparaffinized and digested for 15 min with proteinase K (20 μg/ml) at room temperature. The sections were then treated with 3% H_2O_2 in PBS for 20 min to inactivate endogenous peroxidase. The TdT reaction was performed at 37°C for 90 min. Biotinylated nucleotides were detected using streptavidin–horseradish peroxidase conjugate. Diaminobenzidine staining was performed for 10 min at room temperature, resulting in an insoluble colored substrate at the site of DNA fragmentation. The treated sections were counterstained with methyl green. For quantitative evaluation of the number of TUNEL-positive chondrocytes in the hypertrophic zone, the number of positive cells in the hypertrophic zone was counted and expressed relative to the total number of cells in the hypertrophic zone.

Von Kossa staining

Tibiae and femora of 4-week-old mice (wild type: n = 10, ob/ob: n = 6) and 8-week-old mice (wild type: n = 5, ob/ob: n = 4) were fixed in 10% formalin, embedded in glycol methacrylate and cut into 4-μm sections. Von Kossa staining was performed to visualize the matrix mineralization, and toluidine blue staining was performed to visualize the morphology of chondrocytes. Each image, which contained a scale, was photographed and transferred to a computer. The lengths of the growth plate, resting zone, proliferative zone, non-calcified hypertrophic zone and calcified hypertrophic zone were measured using WinROOF software (Mitani-Corp, Fukui, Japan). The zones were defined as follows: the resting zone, lies immediately adjacent to the secondary bony epiphyses; the proliferative zone, occupied by flattened chondrocytes that are aligned in longitudinal columns; and the hypertrophic zone, occupied by spherical and enlarged chondrocytes [20]. The proportional length of each zone to the whole growth plate was calculated. The proportional length of the calcified hypertrophic zone to the whole hypertrophic zone was also calculated.

Treatment of ob/ob mice with leptin

4-week-old ob/ob mice (n = 4) received intraperitoneal injections of either PBS or 50 μg of recombinant murine leptin (Sigma) in a 150-μl volume once a day. 4-week-old wild-type mice (n = 4) also received PBS for 2 weeks. Then, femora, tibiae and humeri were removed, stained with von Kossa and toluidine blue and analyzed for the extent of matrix mineralization, as described above.

Primary culture of nasal septal chondrocytes and mineralization assay

Chondrocytes were isolated from the nasal septal cartilage of a 2-week-old mouse, following a procedure previously described elsewhere [21]. Briefly, after aseptic dissection of the nasal septal cartilage, tissue fragments were incubated for 2 h at 37°C in an enzymatic mixture of 0.25% collagenase type I (Sigma) and 0.1% hyaluronidase type IVS (Sigma). The cells were centrifuged and resuspended in Dulbecco's modified Eagle medium (DMEM) (Gibco BRL, Gaithersburg, MD, USA) containing 5% FBS, 10 mM β-glycerophosphate (Sigma), 50 μg/ml ascorbic acid (Nakarai tesque, Kyoto, Japan), 50 UI/ml of penicillin and 50 μg/ml streptomycin (Gibco BRL). Mineralization in primary culture was determined by staining with alizarin red S. Plates were washed three times with PBS, then stained with 0.5% alizarin red S in H_2O (pH 5.0) for 1 h at room temperature. After staining, plates were washed three times with H_2O and incubated in 100 mM cetylpyridinium chloride for 1 h to solubilize and release calcium-bound alizarin red S into solution [22]. The absorbance of the released alizarin red S was measured at 570 nm. Data are expressed as units of alizarin red S released (1 unit = 1 unit of optical density at 570 nm) per milligram of protein in each culture. The assay was performed in quadruplicate.

ATDC5 cell culture

The ATDC5 mouse chondrocytic cell line, derived from embryonic carcinoma, was used to assess the in vitro effect of leptin on chondrocytic differentiation. Chondrocytic differentiation culture was performed as described in detail elsewhere [23–25]. Briefly, for the first 3 weeks, cells were cultured in a 1:1 mixture of DMEM/F12 medium containing 5% FBS (Gibco BRL), 10 μg/ml human transferrin (Sigma), 3×10^{-8} M sodium selenite (Sigma) and 10 μg/ml bovine insulin (Sigma) at 37°C in a humidified 5% CO_2/95% air atmosphere. Then, the cells were incubated in α-MEM (Gibco BRL) containing 5% FBS, 10 μg/ml human transferrin, 3×10^{-8} M sodium selenite and 10 μg/ml bovine insulin at 37°C in a humidified 3% CO_2/95% air atmosphere. Cells were cultured for a total of 42 days, with medium replacement every 2 days. In some cultures, recombinant mouse leptin (Sigma) was added at final concentrations of 1 pg/ml to 100 μg/ml. The assay was performed in triplicate.

Northern blotting

Total RNA (20 μg) was subjected to electrophoresis on a 1% agarose gel containing 2.2 M formaldehyde. Then, the RNA was transferred to a nylon membrane using a standard method. The probe was a 0.9-kb fragment of mouse α1(X) collagen cDNA labeled with ^{32}P using the Prime It in vitro transcription kit (Stratagene, La Jolla, CA, USA). Hybridization was performed overnight at 65°C. After hybridization, the membranes were sequentially washed at 45°C: twice with 6× saline sodium citrate (SSC) plus 0.5% sodium dodecyl sulphate (SDS), twice with 2× SSC containing 0.1% SDS and twice with 0.2× SSC containing 0.1% SDS. Hybridization signals were detected with a BAS 2500 BioImage analyzer (Fuji Photo Film, Tokyo, Japan). The Northern blot assay was performed two times.

Flow cytometric analysis of apoptosis and the cell cycle

A flow cytometry apoptosis detection kit (Becton Dickinson, Franklin Lakes, NJ, USA) was used to identify programmed cell death. Cells (1×10^5) were suspended in 100 μl of annexin V binding buffer and were then stained with 10 μl fluorescein isothiocyanate-labeled annexin V (to detect phosphatidylserine expression on cells during early apoptotic phases) and 7-aminoactinomycin (7-AAD) (to exclude dead cells) for 15 min at room temperature in the dark. Then, 400 μl of annexin V binding buffer was added, and at least 10,000 cells were analyzed in a FACScan flow cytometer using CellQuest 3.0.1 software (Becton Dickinson). Percentages of cells undergoing apoptosis were determined by dual-color analysis. We repeated the assay four times. The effect of leptin on the cell cycle of ATDC5 cells was investigated by flow cytometric analysis of cells stained with propidium iodide. Briefly, cells were trypsinized, washed in PBS and fixed in 70% ethanol overnight at 4°C until used. Fixed cells were incubated with 1 mg/ml RNase (Sigma) for 60 min at 37°C. Then, 0.25 mg/ml PI (Sigma) was added for 15 min at 4°C in the dark. We acquired 20,000 cells using FACScalliber (Becton Dick-

Table 1
Femoral, humeral lengths and histomorphometric comparisons of proximal tibial growth plates between wild-type and ob/ob mice

	Wild type (n = 10)	ob/ob (n = 6)	P value[a]
Femoral length (mm)	13.9 ± 0.3	12.3 ± 0.3	0.0046
Humeral length (mm)	12.0 ± 0.1	11.5 ± 0.2	0.0105
Resting zone (%)[b]	9.9 ± 1.9	8.3 ± 1.8	0.2002
Proliferation zone (%)[b]	53.6 ± 3.5	49.1 ± 1.8	0.1495
Non-calcified hypertrophic zone (%)[b]	21.0 ± 3.5	4.4 ± 1.8	0.0039
Calcified hypertrophic zone (%)[b]	15.5 ± 6.0	38.1 ± 0.4	0.0039
Proportional length of calcified zone (%)[c]	43.6 ± 9.4	89.7 ± 9.6	0.0001

Summary of the data from two different experiments was shown.
[a] Statistical differences were analyzed by Mann–Whitney U test.
[b] Proportional length of resting, proliferation, non-calcified hypertrophic or calcified hypertrophic zone (%) represents the ratio of the length of growth plate in tibia.
[c] Proportional length of calcified zone (%) represents the ratio of the length of calcified hypertrophic zone to that of whole hypertrophic zone.

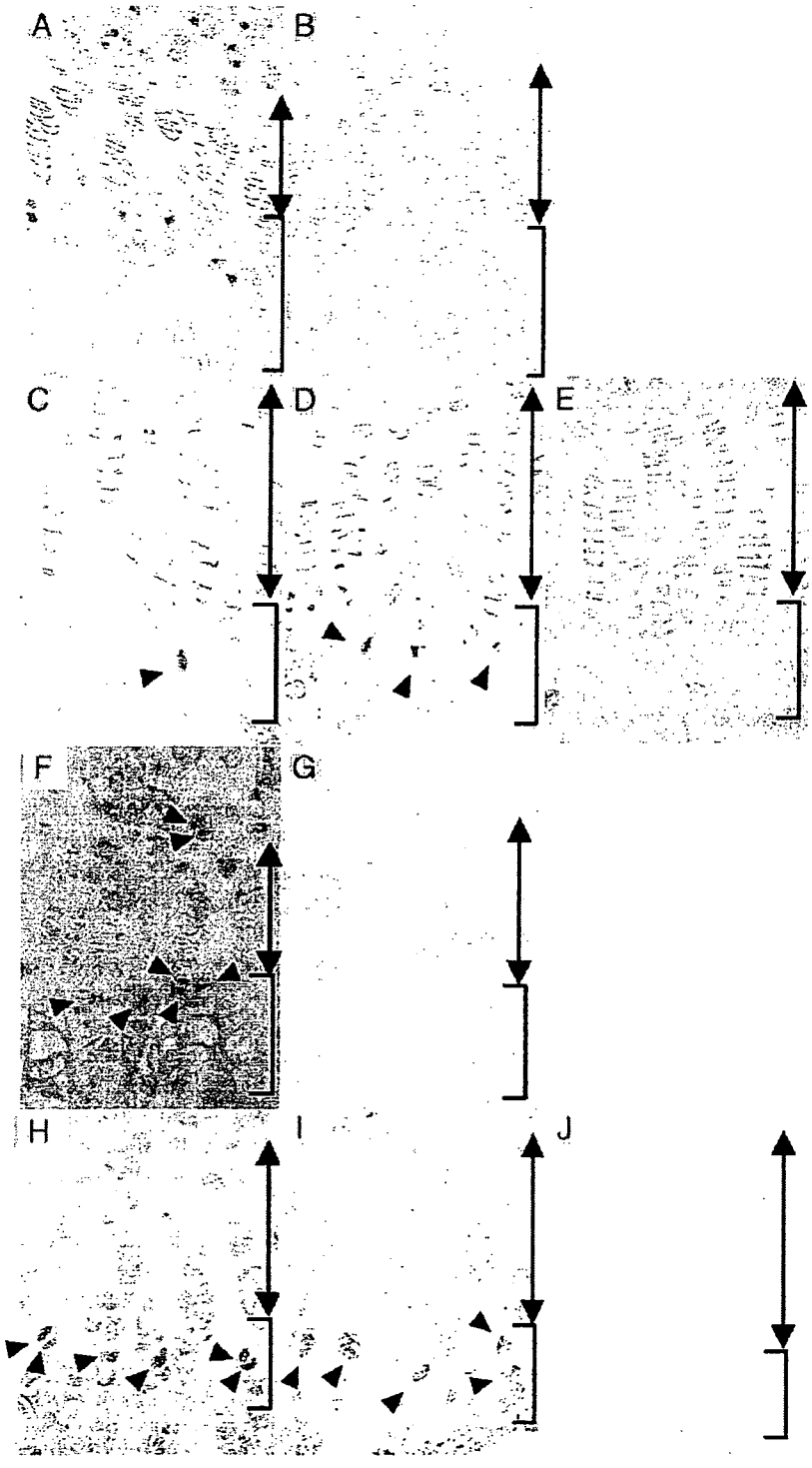

Fig. 1. Immunohistochemical localization of leptin (A, B) and leptin receptor (C, D, E) in the growth plates of 4-week-old wild-type mice (A, C, E) and ob/ob mice (B, D). Leptin expression was identified in resting and prehypertrophic chondrocytes in wild-type mice (A). Ob-Rb was identified in terminal hypertrophic chondrocytes in wild-type (C) and ob/ob (D) mice (arrowheads). (E) Negative controls without primary antibodies. Brackets indicate hypertrophic zones and bidirectional arrows indicate proliferative zones. In situ hybridization of leptin (F, G) and leptin receptor (H, I, J) in the growth plates of 4-week-old wild-type mice (F, H, J) and ob/ob mice (G, I). Expression of leptin mRNA was identified in resting and prehypertrophic chondrocytes in wild-type mice (F) (arrowheads). Ob-Rb mRNA was identified in terminal hypertrophic chondrocytes in wild-type (H) and ob/ob (I) mice (arrowheads). (J) Sense probe. Brackets indicate hypertrophic zones and bidirectional arrows indicate proliferative zones. Magnification: ×400.

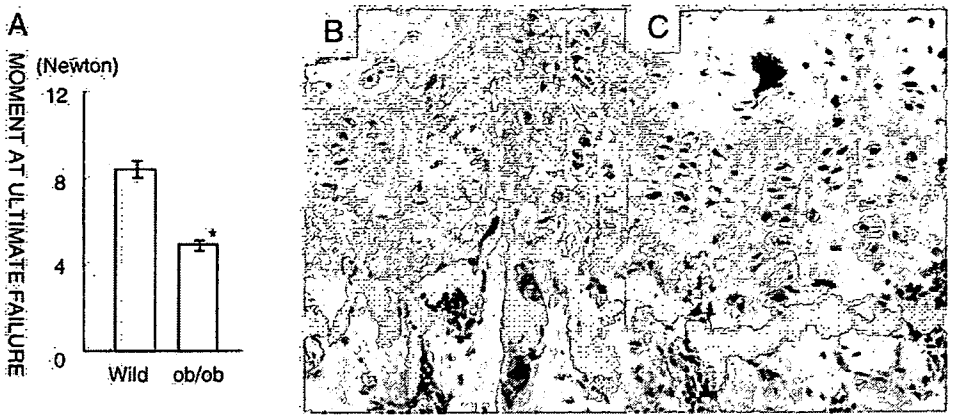

Fig. 2. Mechanical properties of the growth plates. (A) Maximum load required to break the growth plates of 8-week-old wild-type (n = 10) and ob/ob (n = 6) mice. Values are the mean ± SD of the data from two different experiments. Growth plates of ob/ob mice were significantly more fragile than those of wild-type mice (*P = 0.001). (B, C) Histological microphotograph showing that the proximal tibial growth plates of wild-type mouse (B) and ob/ob mouse (C) broke at the chondro-osseous junction. H–E staining. Magnification: ×400.

inson). Data were analyzed using ModFitLT 3.0 software (Becton Dickinson). These experiments were repeated three times. The proliferation index, which is the number of cells in both S and G_2M divided by the total cell number, was calculated.

Measurement of calcium content

Calcium content was measured by the OCPC (ortho-cresolphthalein complexone) method using a calcium C-test Wako kit (Wako Pure Chemical, Tokyo, Japan). First, 200 μl of 2 N hydrochloric acid was added to the wells, followed by shaking at room temperature overnight. Samples were then frozen at −20°C until used. At the time of measurement, 50 μl of sample was added to 5 ml of buffer and 500 μl of substrate. The calcium solution provided in the kit was used to generate a standard curve. The plate was incubated at room temperature for 5 min and then read at 570 nm. We repeated the assay four times.

Statistical analysis

Data are presented as mean ± standard deviation. Groups were compared by analysis of variance (ANOVA) followed by analysis with Fisher's PLSD for multiple comparisons. Individual groups were compared using the Mann–Whitney U test for unpaired analysis. Differences between treatment groups were considered significant at $P < 0.05$.

Results

Ob/ob mice have shorter femora and humeri than wild-type mice

The femora and humeri of 4-week-old wild-type mice and ob/ob mice were measured. The femoral and humeral lengths of ob/ob mice were significantly shorter than those of wild-type mice (Table 1).

Prehypertrophic chondrocytes express leptin and terminal hypertrophic chondrocytes express leptin receptor

The expression of leptin and its receptor in the femora, tibiae and humeri from 4-week-old wild-type mice was examined by immunohistochemistry and in situ hybridization. Leptin mRNA and protein expression was observed in resting and prehypertrophic chondrocytes in the growth plates of wild-type mice (Figs. 1A and F). No leptin expression was detected in the proliferative or hypertrophic zone. Positive staining for leptin receptor mRNA and protein was observed in terminal hypertrophic chondrocytes in both wild-type and ob/ob mice (Figs. 1C, D, H and I).

Fig. 3. Histological and histochemical analyses of 4-week-old wild-type mice and ob/ob mice. (A–D) Von Kossa and toluidine blue double staining of tibiae of wild-type mice (A, C) and ob/ob mice (B, D). In wild-type mice, the proportional length of calcified hypertrophic zone to whole hypertrophic zone was less than 50%. However, in ob/ob mice, most part of hypertrophic zone was mineralized. The column structure of proliferating and hypertrophic chondrocytes was also disturbed. Brackets indicate the entire hypertrophic zone, and bidirectional arrows indicate the calcified hypertrophic zone. Magnifications: ×100 (A, B) and ×400 (C, D). (E, F) The expression level of type X collagen in the growth plates of femora and humeri of 4-week-old wild-type mice (n = 4) and ob/ob (n = 4) mice. The amplified PCR products were 459 base pair (bp) for type X collagen and 307 bp for G3PDH (E). Real-time PCR analyses of expression level of type X collagen in the femoral and humeral growth plates of wild-type mice and ob/ob mice (F). Values are given as mean ± SD. Type X collagen expression in growth plates of ob/ob mice was significantly less than that of wild-type mice (*P = 0.0357). (G, H) Electron microscopy images of the hypertrophic zone of wild-type mice (G) and ob/ob mice (H). In wild-type mice, collagen fibrils ran parallel to one another, whereas in ob/ob mice, collagen fibrils showed less-organized loose reticular arrangement. Magnification: ×30,000. (I, J) TUNEL staining of the hypertrophic zone of wild-type mice (I) and ob/ob mice (J). The percentage of hypertrophic chondrocytes that were TUNEL positive was greater in ob/ob mice than in wild-type mice.

Ob/ob mice have fragile growth plates

The growth plates of ob/ob mice were significantly more fragile than those of wild-type mice (Mann–Whitney U test, $P = 0.001$). The average force at ultimate failure was 8.4 ± 1.5 N for wild-type segments and 4.9 ± 0.6 N for ob/ob segments (Fig. 2A). After the mechanical test, all samples were processed for histological examination. The breakage occurred at the chondro-osseous junction in all tibiae regardless of the genotype (Figs. 2B and C).

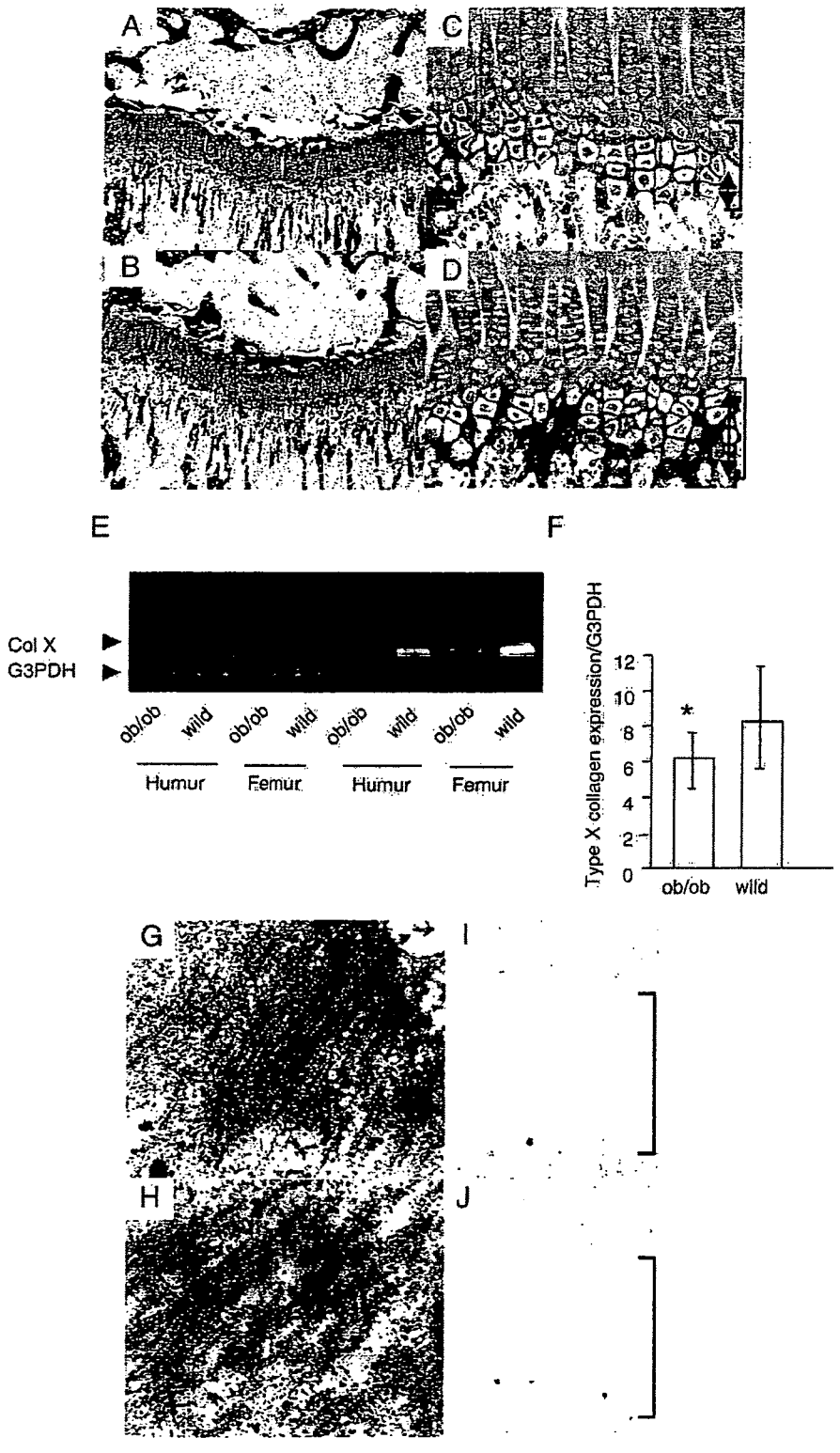

Alterations in morphology, mineralization, type X collagen expression, matrix microstructure and chondrocyte apoptosis in the growth plates of ob/ob mice

Higher magnification of eosin-stained and von Kossa-stained sections revealed that the column structure of proliferating and hypertrophic chondrocytes was disturbed. The majority of the columns in ob/ob mice seemed to be bent or twisted, and the chondrocytes were poorly aligned. In some columns, chondrocytes were distributed like pebble stones rather than a column. Matrix mineralization was also altered in 4-week-old ob/ob mice. In wild-type mice, the proportional length of the calcified hypertrophic zone to the whole hypertrophic zone was less than 50% (Figs. 3A and C; Table 1). However, in ob/ob mice, most of the hypertrophic zone was mineralized (Figs. 3B and D; Table 1). The proportional length of the calcified hypertrophic zone to the whole hypertrophic zone in the ob/ob mice was significantly greater than that of wild-type mice (Table 1, Mann–Whitney U test, $P = 0.0001$), whereas there was no detectable difference in the proportional length of the other zones to the growth plate.

In situ hybridization assays found no difference in mRNA expression of type II or type X collagen in wild-type and ob/ob mice (data not shown). However, the expression level of type X collagen in the growth plates of ob/ob mice was lower than that in wild-type mice (Fig. 3E). Real-time PCR showed that the expression level of type X collagen in ob/ob mice was 0.48-fold the expression level in wild-type mice (ob/ob mice: 4.4 ± 2.7; wild-type mice: 9.2 ± 7.4%; Mann–Whitney U test, $P = 0.0357$) (Fig. 3F).

We examined the collagen fibril microstructure in the hypertrophic zone by transmission electron microscopy. There was no significant difference in the diameter of collagen fibrils from 4-week-old wild-type mice and ob/ob mice (data not shown). However, electron microscopy of the hypertrophic zone of 4-week-old ob/ob mice revealed a less-organized loose reticular distribution of collagen fibrils (Fig. 3H), in contrast to the well-organized parallel collagen fibrils in wild-type mice (Fig. 3G).

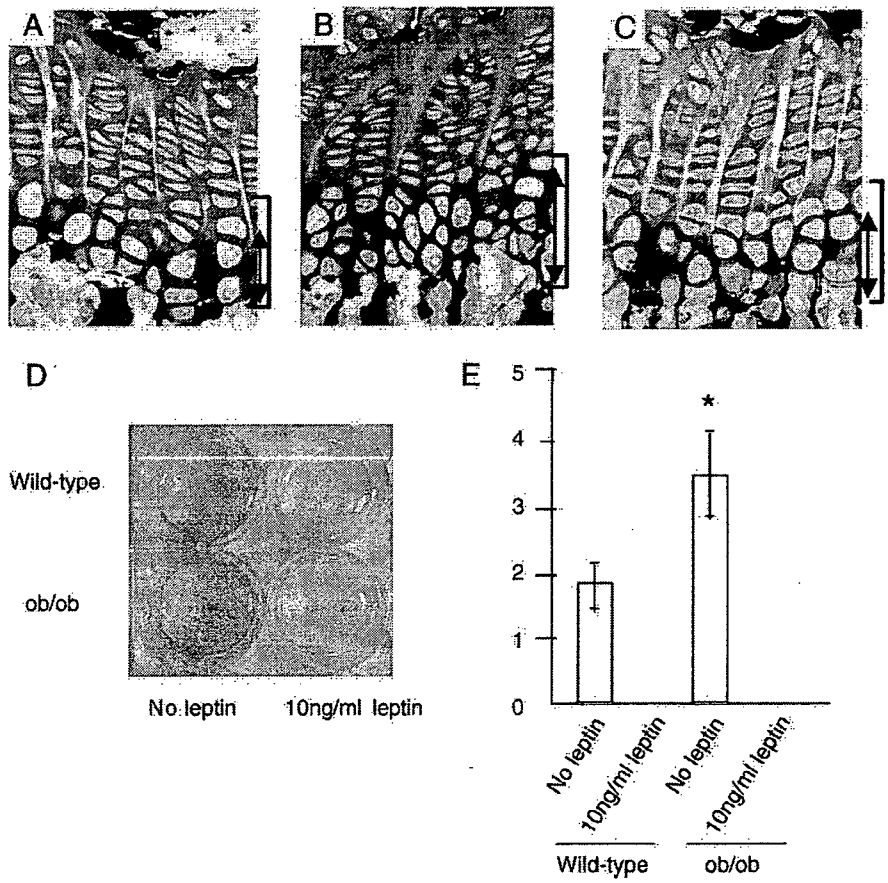

Fig. 4. Cartilage matrix mineralization in ob/ob mouse and the effect of leptin treatment. (A, B, C) Von Kossa/toluidine blue double staining of tibial growth plates of wild-type mice treated with PBS (A), ob/ob mice with PBS (B) and ob/ob mice with leptin (C) for 2 weeks. Brackets indicate whole hypertrophic zones and bidirectional arrows indicate calcified hypertrophic zones. Magnification: ×400. (D, E) Mineralization in primary culture of nasal septal chondrocytes of wild-type mice and ob/ob mice. Mineral deposit was stained by alizarin red S (D) and quantified the absorbance of the solubilized alizarin red S at 570 nm (E) as described in Material and methods. The assay was performed in quadruplicate. Values are given as mean ± SD. On days 17, mineralization occurred in the both types of cells without leptin, whereas no mineralization was found in cultures with leptin (D). A quantitative analysis revealed that matrix mineralization in cultures of ob/ob chondrocytes without leptin was significantly more than others than others (ANOVA, $^*P < 0.0001$).